Cardiac myosin binding protein C regulates postnatal myocyte cytokinesis

Jianming Jiang[a,b,c,1], Patrick G. Burgon[a,d,1], Hiroko Wakimoto[a,e,1], Kenji Onoue[a,1], Joshua M. Gorham[a], Caitlin C. O'Meara[f], Gregory Fomovsky[f], Bradley K. McConnell[a,g], Richard T. Lee[f], J. G. Seidman[a,2,3], and Christine E. Seidman[a,b,f,2]

[a]Department of Genetics, Harvard Medical School, Boston, MA 02115; [b]Howard Hughes Medical Institute, Harvard Medical School, Boston, MA 02115; [c]Department of Biochemistry and Cardiovascular Research Institute, Yong Loo School of Medicine, National University of Singapore, Singapore 117599; [d]University of Ottawa Heart Institute, Ottawa, ON K1Y 4W7, Canada; [e]Department of Cardiology, Children's Hospital Boston, Boston, MA 02115; [f]Division of Cardiovascular Medicine, Brigham and Women's Hospital, Boston, MA 02115; and [g]Department of Pharmacological and Pharmaceutical Sciences, University of Houston, Texas Medical Center, Houston, TX 77204

Contributed by J. G. Seidman, June 11, 2015 (sent for review January 30, 2015; reviewed by Sharlene M. Day)

Homozygous cardiac myosin binding protein C-deficient (Mybpc$^{t/t}$) mice develop dramatic cardiac dilation shortly after birth; heart size increases almost twofold. We have investigated the mechanism of cardiac enlargement in these hearts. Throughout embryogenesis myocytes undergo cell division while maintaining the capacity to pump blood by rapidly disassembling and reforming myofibrillar components of the sarcomere throughout cell cycle progression. Shortly after birth, myocyte cell division ceases. Cardiac MYBPC is a thick filament protein that regulates sarcomere organization and rigidity. We demonstrate that many Mybpc$^{t/t}$ myocytes undergo an additional round of cell division within 10 d postbirth compared with their wild-type counterparts, leading to increased numbers of mononuclear myocytes. Short-hairpin RNA knockdown of *Mybpc3* mRNA in wild-type mice similarly extended the postnatal window of myocyte proliferation. However, adult Mybpc$^{t/t}$ myocytes are unable to fully regenerate the myocardium after injury. MYBPC has unexpected inhibitory functions during postnatal myocyte cytokinesis and cell cycle progression. We suggest that human patients with homozygous *MYBPC3*-null mutations develop dilated cardiomyopathy, coupled with myocyte hyperplasia (increased cell number), as observed in Mybpc$^{t/t}$ mice. Human patients, with heterozygous truncating *MYBPC3* mutations, like mice with similar mutations, have hypertrophic cardiomyopathy. However, the mechanism leading to hypertrophic cardiomyopathy in heterozygous *MYBPC3*$^{+/-}$ individuals is myocyte hypertrophy (increased cell size), whereas the mechanism leading to cardiac dilation in homozygous *Mybpc3*$^{-/-}$ mice is primarily myocyte hyperplasia.

myosin binding protein C | cardiac dilation | cardiac hypertrophy | cytokinesis | hyperplasia

Dilated cardiomyopathy (DCM) leads to heart failure and is a leading cause of morbidity and mortality (1, 2). DCM is generally diagnosed as left ventricular (LV) dilation with associated reduction in cardiac contraction measured as impaired fractional shortening (3). Hearts from affected individuals frequently demonstrate myocyte elongation, myocyte death, and fibrosis, in addition to LV dilation. DCM results from a variety of environmental factors, such as viral infection and alcohol abuse, as well as from mutations in a number of genes including titin, lamin A/C, cardiac actin, cardiac myosin heavy chain, and phospholamban (reviewed in refs. 4–6). Whether all of these DCM-inducing factors activate the same or different cellular pathways to produce similar clinical features remains uncertain. The mechanisms by which mutations in the cardiac myosin binding protein C (*MYBPC3*) gene and other sarcomere protein genes lead to cardiac dilatation are under investigation.

MYBPC is a thick filament accessory protein component of the striated muscle sarcomere A band that constitutes 2–4% of the myofibril (discussed in ref. 7). Although there are four *Mybpc* genes in the mammalian genome, only cardiac *Mybpc* (*Mybpc3*) is expressed in embryonic, neonatal, and adult hearts (8, 9). Cardiac MYBPC interacts with at least four sarcomere components: myosin heavy chain, actin, myosin light chain 2, and titin (10–12). More than 400 cardiac *MYBPC3* gene mutations have been identified in patients as a cause of hypertrophic cardiomyopathy (HCM), an autosomal dominant disorder resulting from defective sarcomeres (for reviews, see refs. 12, 13). Due to an ancient founder mutation, 4% of the population of India carries a truncating *MYBPC3* mutation (14, 15). The majority of cardiac *MYBPC3* mutations are predicted to encode truncated proteins that lack portions of either the carboxyl myosin and/or titin binding domains (7, 13). These truncating *MYBPC3* mutations are thought to cause cardiac hypertrophy by inducing myocyte hypertrophy (increased cell size), rather than myocyte hyperplasia.

We and other researchers have created mice that carry a mutant cardiac *Mybpc3* gene to create murine HCM models (16–18). Heterozygous mice, designated Mybpc$^{t/+}$, like humans bearing the same mutation, develop adult onset HCM. Homozygous *MYBPC3* mutations are a much rarer cause of human DCM than autosomal dominant mutations in other sarcomere protein genes. However, homozygous Mybpc$^{t/t}$ mice that express two mutant alleles and no wild-type cardiac *Mybpc3* develop LV dilation by 3 d postbirth and have all of the features of DCM, including LV chamber dilation, albeit mildly impaired fractional

Significance

We demonstrate that hearts lacking the sarcomere protein cardiac myosin binding protein C (MYBPC) undergo altered development due to an extra round of postnatal cell division. Normal cardiac myocytes replicate rapidly during fetal life, undergo a final round of cell division shortly after birth, cease dividing, and increase in cell size during prepubescent life. MYBPC has an unexpected function—inhibition of myocyte cytokinesis. MYBPC-deficient myocytes undergo an additional round of cytokinesis, resulting in increased numbers of myocytes and a greater proportion of mononuclear myocytes in neonatal hearts. Our findings provide insights into the mechanisms of dilated cardiomyopathy caused by homozygous mutations that reduce MYBPC levels.

Author contributions: J.J., P.G.B., H.W., B.K.M., R.T.L., J.G.S., and C.E.S. designed research; J.J., P.G.B., H.W., K.O., J.M.G., C.C.O., G.F., and B.K.M. performed research; H.W., K.O., and J.M.G. contributed new reagents/analytic tools; J.J., P.G.B., H.W., K.O., J.M.G., C.C.O., B.K.M., R.T.L., J.G.S., and C.E.S. analyzed data; and J.J., P.G.B., H.W., J.G.S., and C.E.S. wrote the paper.

Reviewers included: S.M.D., University of Michigan.

The authors declare no conflict of interest.

[1]J.J., P.G.B., H.W., and K.O. contributed equally to this work.

[2]J.G.S. and C.E.S. contributed equally to this work.

[3]To whom correspondence should be addressed. Email: seidman@genetics.med.harvard.edu.

This article contains supporting information online at www.pnas.org/lookup/suppl/doi:10.1073/pnas.1511004112/-/DCSupplemental.

shortening (16). Unlike most humans with DCM, homozygous mutant cardiac Mybpc$^{t/t}$ mice have normal survival despite their cardiac disease. Other homozygous null cardiac *Mybpc3* mice develop an identical phenotype (7, 17, 18). Hence, for the studies described here, we assume that the phenotype of the Mybpc$^{t/t}$ mice is due to lack of MYBPC protein, rather than to small amounts of truncated protein. Recently, two groups have demonstrated that delivery of MYBPC to *Mybpc3*-null hearts restores cardiac function and morphology (19, 20). Here, we have begun to dissect the mechanism by which homozygous Mybpc$^{t/t}$ hearts develop DCM.

Because Mybpc$^{t/t}$ mice begin LV dilation within a few days postbirth (16), we hypothesized that this reflected abnormal development of neonatal myocytes. During fetal and early perinatal development in wild-type hearts, cardiomyocytes divide rapidly, producing hyperplastic cardiac growth (21). However, at 10 d postbirth, cardiomyocytes cease to divide and all subsequent increases in myocardial mass result from myocyte hypertrophy (22). Despite the importance of this phenomenon, little is known about the molecular basis for the transition from hyperplasic to hypertrophic-based myocardial growth. We hypothesized that abnormal cardiomyocyte growth, either hyperplastic or hypertrophic, in the perinatal period accounted for the LV dilation of Mybpc$^{t/t}$ mouse hearts. To address this question, we have counted and measured cardiomyocytes from Mybpc$^{t/t}$ and wild-type mice. We have also studied the consequences of reducing MYBPC levels by injecting *Mybpc3*-specific shRNA at birth. Neonatal cardiomyocytes lacking cardiac MYBPC, due to *Mybpc3*-specific shRNA knockdown, undergo an additional round of cytokinesis. We conclude that dramatic reductions in the amount of cardiac MYBPC leads to aberrant cell cycle regulation at the G1/S checkpoint, resulting in at least one extra round of myocyte division and DCM.

Results

Increased Numbers and Immaturity of Cardiac Myocytes in Mybpc$^{t/t}$ Mice. Cardiac tissues and myocytes from wild-type and Mybpc$^{t/t}$ mice were studied from birth to postnatal day 35 (designated as P0–35). The hearts from P5 Mybpc$^{t/t}$ mice had a significantly increased LV mass and LV/body weight ratio compared with wild-type mice (Fig. 1 *A* and *B* and Fig. S1*A*). Myocytes from P3 and P10 Mybpc$^{t/t}$ mice were 20–30% wider than wild-type myocytes (Fig. S1 *B* and *C*), which we presume reflects myocyte immaturity (23) and/or abnormal spacing between parallel sarcomeres due to MYBPC deficiency (24). There was no significant difference in the length of myocytes from wild-type and Mybpc$^{t/t}$ mice (Fig. S1*D*).

As expected (22, 25, 26), nearly all wild-type adult LV myocytes were binuclear (Fig. 1 *C–E*). Analyses of younger mice confirmed this finding. At P21, ~5% of wild-type and heterozygous Mybpc$^{t/+}$ LV myocytes were mononuclear and 90% were binuclear (Fig. 1*E*). However, significantly less Mybpc$^{t/t}$ LV myocytes were binuclear (Fig. 1*E*; WT:Mybpc$^{t/+}$:Mybpc$^{t/t}$, 89.8%:89.7%:74.8%; $P = 0.0003$). Consistent with this observation was the observation that ~threefold more Mybpc$^{t/t}$ LV myocytes were mononuclear than either wild-type or heterozygous Mybpc$^{t/+}$ LV myocytes (Fig. 1*E*; WT:Mybpc$^{t/+}$:Mybpc$^{t/t}$, 5.8%:6.7%:18.3%; $P < 4E\text{-}5$). We defined myocyte numbers and nuclear morphology in hearts from 5-wk-old Mybpc$^{t/t}$ and wild-type mice by immunohistochemical staining of 10 sections evenly distributed across the LV. Wheat germ agglutinin (WGA) was used to demarcate plasma membrane boundaries (Fig. 2 *A* and *B*), and nonmyocytes were excluded by size and absence of cardiac troponin I staining. In comparison with wild-type, Mybpc$^{t/t}$ LV contained ~40% more myocytes than wild-type LV (Fig. 2*C*; $P = 0.006$).

Previous studies have demonstrated that by P10 the majority of wild-type binuclear myocytes have exited the cell cycle (27). We hypothesized that the increased proportion of mononuclear to binuclear myocytes in Mybpc$^{t/t}$ hearts reflected either premature cell cycle arrest before becoming binuclear or alternatively that mutant myocytes had continued cell cycle progression with cytokinesis—a delay in cell cycle exit that would account for greater myocyte number. To distinguish these models, we used three approaches to study cell cycle progression.

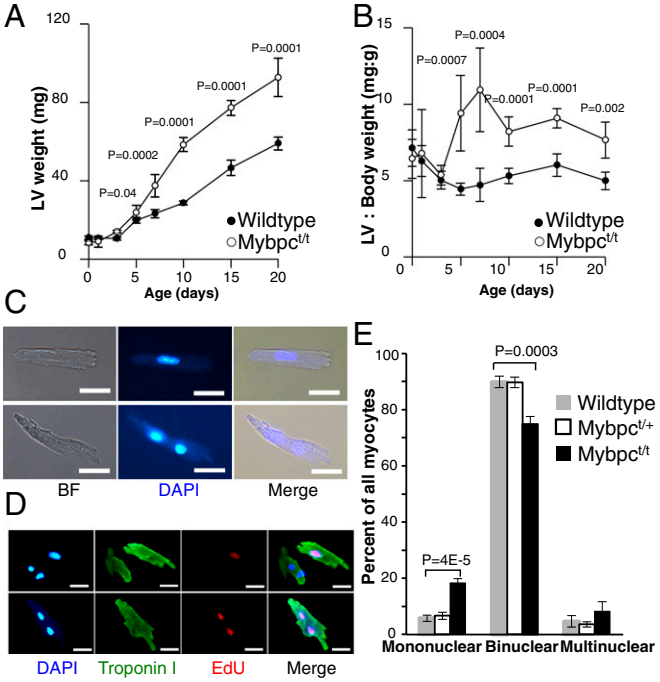

Fig. 1. LV mass and myocyte nucleation in wild-type and Mybpc$^{t/t}$ hearts. (*A* and *B*) Changes in LV mass (*A*) and LV weight/body weight ratios (*B*) of wild-type (filled circle) and Mybpc$^{t/t}$ (open circle) mice from P0–20 (n = 5–10 neonates per time point). (*C*) Light micrographs of DAPI-stained isolated mononuclear (*Upper* panel) and binuclear (*Lower* panel) myocytes from 3-wk-old Mybpc$^{t/t}$ mice visualized with bright field (BF) and fluorescent (DAPI) illumination. (Scale bar, 20 μm.) (*D*) Representative light micrographs of isolated LV myocytes from EdU-labeled Mybpc$^{t/t}$ mice that are stained for nuclei (blue), troponin I (green), and EdU (red). A mononuclear myocyte (arrows) is indicated. (Scale bar, 20 μm.) (*E*) Distribution of mononuclear, binuclear, and multinuclear myocytes from 3-wk-old wild-type (gray), Mybpc$^{t/+}$(white box), and Mybpc$^{t/t}$ (black) hearts. Data are presented from four mice per genotype, 200–300 cells per mouse (mean ± SD). All *P* values reflect comparison of wild-type and Mybpc$^{t/t}$ hearts.

Mybpc$^{t/t}$ Myocytes Have Delayed Cell Cycle Exit. We injected the thymidine analog 5-ethynyl-2'-deoxyuridine (EdU) (28) into wild-type and Mybpc$^{t/t}$ neonates at P1 through P5 and assessed DNA synthesis in isolated P14 myocytes (Fig. 1*D*). In comparison with wild type, there were significantly more EdU-positive mono- and binuclear myocytes from Mybpc$^{t/t}$ mice (47.02 ± 2.50% vs. 29.35 ± 3.06%; $P = 0.0003$; four mice per genotype; 200–300 cells per mouse). To identify cells undergoing mitosis, we used an anti-histone H3 phosphorylation (pH3) antibody that detects pH3 of serine residue 10 during the mitotic (M) phase of the cell cycle (29). Immunohistochemistry analyses of pH3 at P3, P7, and P10 (Fig. 3 *A* and *B*) indicated almost twice as many myocytes undergoing mitosis in Mybpc$^{t/t}$ than in wild-type hearts. Finally, we performed immunostaining for Aurora B kinase (Aurora B), which localizes to the central spindle during anaphase and in the midbody during cytokinesis (30). As cell cycle exit is arrested before cytokinesis during normal neonatal myocyte development, Aurora B kinase was rarely detected in the central spindle or midbody of wild-type myocytes. In contrast, P7 Mybpc$^{t/t}$ myocytes had 15-fold more Aurora B staining, which

DEVELOPMENTAL BIOLOGY

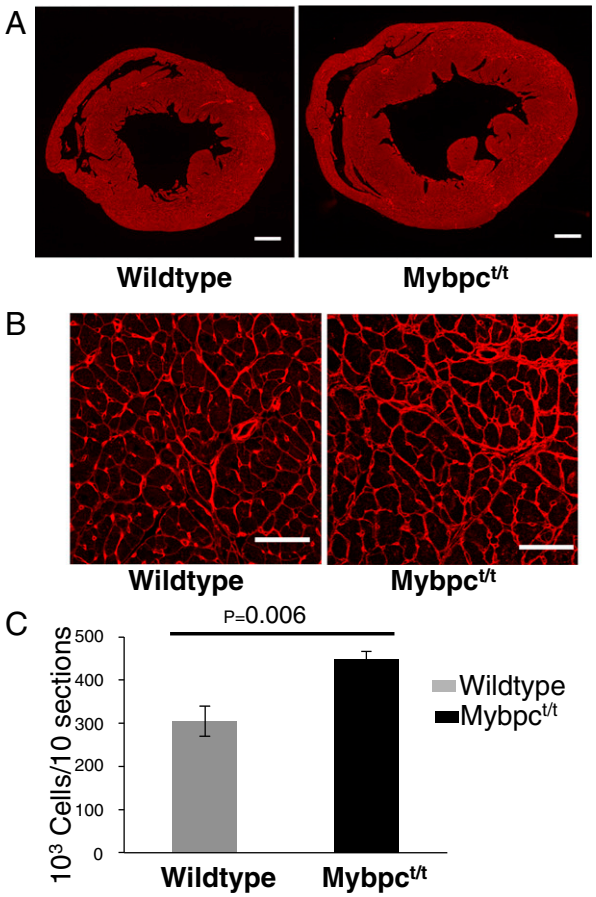

Fig. 2. Increased numbers of myocytes in Mybpc$^{t/t}$ compared with wild-type hearts. (*A* and *B*) Transverse heart sections stained with WGA at low (*A*; scale bar, 0.5 mm) and high (*B*; scale bar, 50 μm) magnification. (*C*) Quantification of myocytes from wild-type (gray) and Mybpc$^{t/t}$ (black) mice. Data are presented from three mice per genotype, 10 sections per mouse (mean ± SD).

was localized to the cytoplasmic bridge between daughter cells (Fig. 3 *C* and *D*). Based on the increase in EdU incorporation and pH3 and Aurora B immunostaining in Mybpc$^{t/t}$ mice, we concluded that mutant myocytes have delayed cell cycle exit during neonatal life and undergo additional rounds of cell division. As a result, Mybpc$^{t/t}$ mice had both more myocytes and more mononuclear myocytes than wild-type hearts.

To further assess cell cycle regulation in neonatal (P10) Mybpc$^{t/t}$ LV, we assessed expression of cell cycle-related genes by RNAseq (Table S1). One hundred and seven genes that are described as "cell division," "cyclin-associated," or "cell cycle" genes are expressed in the wild-type P10 LV. Expression of 70 cell cycle-related genes either increased or decreased ($P < 0.001$), whereas 38 of the cell cycle-related genes were expressed at similar levels in wild-type and Mybpc$^{t/t}$ LV. Presumably these cell cycle-associated gene expression changes are related to changes in cell cycle exit found in neonatal Mybpc$^{t/t}$ LV.

Neonatal Depletion of Cardiac MYBPC Impairs Myocyte Maturation in Wild-Type Mice. To confirm that altered myocyte maturation in Mybpc$^{t/t}$ hearts was due to the myocyte-autonomous deficiency of MYBPC, we used the cardiotropic adeno-associated virus serotype 9 (AAV9) (31, 32) to deliver *Mybpc3*-specific shRNA to the neonatal heart. Two *Mybpc3*-specific shRNAs that targeted different regions of *Mybpc3* RNA (Fig. S2*A*) were constructed with a colinear EGFP reporter gene downstream of the cardiac troponin T (cTnT) promoter, so as to exclude nonmyocyte expression (Fig. S2*B*).

AAV9-Mybpc3-shRNA was injected into the thoracic cavity of P1 wild-type neonates [5×10^{13} viral genomes (vg)/kg], and EGFP fluorescence was assessed to monitor shRNA expression. Cardiac EGFP fluorescence was detected 48 h after virus injection and continued for at least 5 mo (Fig. 4*A*) but was absent from all other organs (33). EGFP fluorescence was present in 60–80% of adult myocytes isolated from viral-transduced mice (Fig. 4*B*). Both of these shRNA constructs (denoted AAV9-Mybpc3-shRNA) had comparable efficiency in attenuating in vivo *Mybpc3* RNA expression (Fig. 4*C*).

Four weeks after viral injection, EGFP-positive myocytes were isolated, and nuclear morphology was examined. Wild-type mice infected with a control shRNA (that targeted LacZ RNA; *Materials and Methods*) had ∼5% mono- and 90% binuclear myocytes (Fig. 4*D*). Among EGFP-positive myocytes, wild-type hearts injected with Mybpc3-specific shRNA had 5–6-fold more mononuclear myocytes than hearts injected with control shRNA (Fig. 4*D*). Mice infected with either of the two distinct Mybpc3-specific shRNA constructs showed similar results (Fig. 4*D*).

Myocyte Proliferation After Cardiac Injury in Mybpc$^{t/t}$ Mice. We considered whether Mybpc$^{t/t}$ mice have better cardiac regenerative capacity after injury than wild-type mice, as myocyte division may play an important role in regeneration. To test this hypothesis, we performed sham or LV apical resections (26, 34), excising ∼15% of the total LV mass in P10 wild-type and Mybpc$^{t/t}$ mice (Fig. 5 *A*–*I*). There is no difference in survival of the two genotypes after apical resection. Surviving neonates received a BrdU pulse 1 d later, and at P17 BrdU incorporation was assessed in hearts stained with cTnT-specific antibody, to exclude nonmyocytes, and with Ki67 antibody to detect cell cycle activity (Fig. 5 *J* and *K*). Sections from sham-operated Mybpc$^{t/t}$ LV (47 ± 5 BrdU$^+$;cTnT$^+$ cells/mm^2) had significantly more cTnT-positive, BrdU-labeled cells than sham-operated wild-type hearts (5 ± 0 BrdU$^+$;cTnT$^+$ cells/mm^2; $P = 0.005$) or Ki67-labeled (18 ± 8 Ki67$^+$;cTnT$^+$ cells/mm^2 vs. 3 ± 3 Ki67$^+$;cTnT$^+$ cells/mm^2; $P = 0.05$; Fig. 5 *J* and *K*). Apical resection did not increase BrdU incorporation into cTnT-positive cells from either wild-type and Mybpc$^{t/t}$ mice, and Ki67 staining was not increased in either wild-type or Mybpc$^{t/t}$ LV (Fig. 5 *J* and *K*).

Notably, dystrophic calcification, a marker of cell death and necrosis, was observed in apical resected regions in all Mybpc$^{t/t}$ mice, but not in apical resected wild-type or sham-operated Mybpc$^{t/t}$ mice (Fig. 5 *B*, *H*, and *I*). As cTnT-positive cells without nuclei surrounded these necrotic foci, we deduced that Mybpc$^{t/t}$ myocytes were particularly sensitive to dystrophic calcification and death. The demise of Mybpc$^{t/t}$ myocytes was unlikely to reflect inadequate vascular supply, as staining by the vascular endothelial marker CD31 was comparable in wild-type and Mybpc$^{t/t}$ mice (Fig. S3). Dystrophic calcification also occurred in both apical and basal regions when apical resection was carried out in P1 Mybpc$^{t/t}$ mice (Fig. S4). We suggest that Mybpc$^{t/t}$ hearts were more susceptible to necrotic death after resection due to altered biomechanical properties that increased energy requirements due to enhanced actomyosin force (35) and/or elevated wall stress (24) in Mybpc$^{t/t}$ myocytes. Mybpc$^{t/t}$ mice appear to have reduced regenerative capacity compared with wild-type mice.

Discussion

MYBPC is critical for normal cardiac structure and function. Absence of MYBPC in the adult heart compromises the stiffness and rigidity of myofilaments (36, 37), reduces sarcomere packing density (24), and perturbs contractile performance (16), which might account for increased myocyte width in Mybpc$^{t/t}$ mice and contribute to increased LV wall thickness (Fig. S1 *C* and *D*). We show that MYBPC also has unexpected roles in postnatal maturation of myocytes. Postnatal Mybpc$^{t/t}$ myocytes appear morphologically

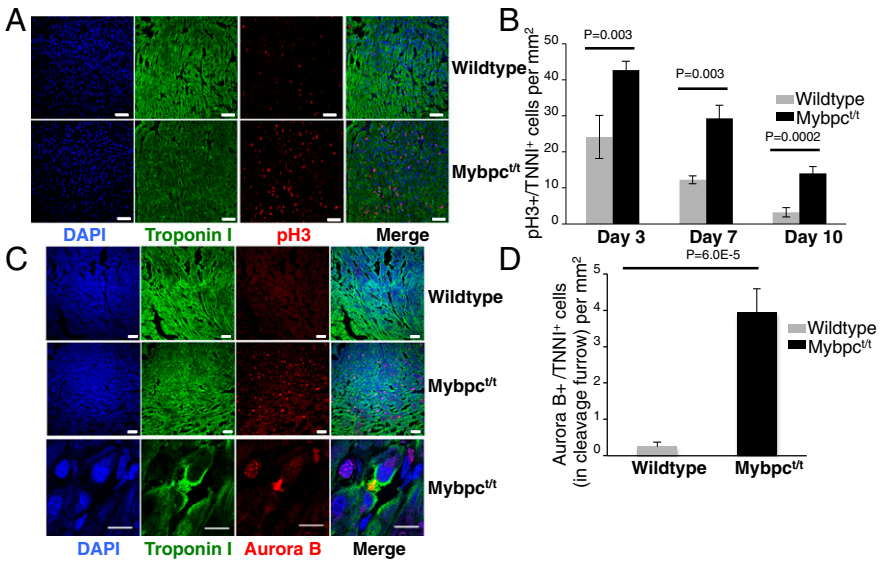

Fig. 3. pH3 and Aurora B expression in wild-type and Mybpc$^{t/t}$ hearts. (*A*) Confocal micrographs of P7 wild-type and Mybpc$^{t/t}$ LV sections stained with DAPI (blue), troponin I (green), and pH3 (red). (Scale bar, 20 μm.) (*B*) Quantification of pH3-positive myocytes in wild-type (gray) and Mybpc$^{t/t}$ (black) hearts from P3, P7, and P10 mice. Data are presented from four mice per genotype, three sections per mouse (mean ± SD). (*C*) Confocal micrographs of cardiac sections from P7 wild-type and Mybpc$^{t/t}$ mice stained with DAPI (blue), troponin I (green), and Aurora B (red). [Scale bar, (*Upper*) 20 μm and (*Lower*) 5 μm.] (*D*) Quantification of Aurora B located at the bridge of two daughter myocytes in wild-type (gray) and Mybpc$^{t/t}$ (black) hearts from P7 mice. Data are presented from four mice per genotype, three sections per mouse (mean ± SD).

immature, based on dimensions and a single nucleus, unlike postnatal wild-type myocytes. During neonatal development, Mybpc$^{t/t}$ myocytes undergo additional rounds of division, resulting in increased myocyte numbers in Mybpc$^{t/t}$ hearts (Fig. 6). Given its established role in myofilament lattice rigidity (1, 7, 12, 17, 18, 24), we conclude that MYBPC is critical for inhibiting postnatal myocyte cytokinesis, an essential step in myocyte maturation accompanying cell cycle exit.

To progress through the cell cycle, myocytes must disassemble both the cytoskeleton and the contractile apparatus, the thick and thin myofilaments of the sarcomere. High-resolution confocal microscopy of immunostained neonatal myocytes has identified two phases of sarcomere dissolution. Before metaphase, proteins in the z disk and thin filament disassemble, whereas thick filament proteins, including myosin and MYBPC, maintain a mature, cross-striated pattern. Late in anaphase, thick filament proteins disassemble and remain dispersed until cytokinesis is complete (38).

Before cell cycle exit, neonatal mouse myocytes undergo karyokinesis without cytokinesis (39, 40). This phase in myocyte maturation is characterized by synchronized changes in the expression of cell cycle molecules; levels of activators (Cdk2, Cdk3, Cdk4, Cdk cofactors, and Ccnd1) are decreased, and levels of inhibitors (p21, p27KIP1, TSC2, p130, and Rb) are increased. Transgenic overexpression or genetic depletion in the heart of some cell cycle regulators (27, 41) has been demonstrated to partially overcome neonatal myocyte cell cycle arrest and enable additional rounds of cell division. Recent studies demonstrate that these reciprocal events are mediated in part by the transcriptional activator 14-3-3ε (42), the transcription factor Meis1 (43), and activation of the DNA damage response pathway induced by reactive oxygen species in neonatal mice (44).

MYBPC deficiency also impacted the regenerative capacity of the P10 mouse heart. Apical resection did not increase BrdU incorporation or Ki67 staining among cTnT-positive cells in Mybpc$^{t/t}$ mice as it did in wild-type mice (Fig. 5 and Fig. S3). Moreover, as resected Mybpc$^{t/t}$ hearts showed necrosis and dystrophic calcification, we suspect that MYBPC-deficient myofilaments are less resistant to sheer forces and perhaps more susceptible to depolymerization, as has been seen ex vivo (36, 45). These observations hint at the dichotomy inherent in a rigid sarcomere, a structure that can support the stress of contraction but that also impedes myocyte regeneration.

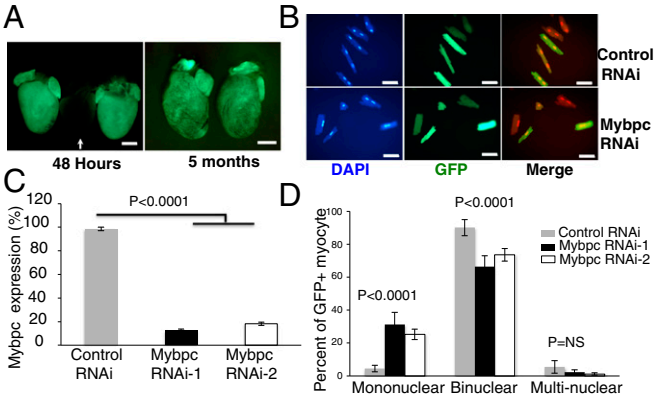

Fig. 4. Depletion of *Mybpc3* RNA by AAV-shRNA. (*A*) Hearts from three wild-type mouse hearts harvested 48 h after transduction with AAV9 lacking EGFP (center, arrow) or with AAV9-EFFP (two flanking center heart) visualized under fluorescent light. *Right* panel shows two hearts harvested 5 mo after AAV9-EFFP transduction. (Scale bar, 2 mm.) (*B*) Fluorescent microscopy of LV myocytes stained by DAPI (blue) and EGFP (green) isolated from wild-type mice transduced with AAV-LacZ shRNA (control, *Upper* panels) or AAV-Mybpc3 shRNA (*Lower* panels). DAPI was shown in red in merged images. (Scale bar, 50 μm.) (*C*) Quantitative real-time PCR analysis of LV *Mybpc3* expression from mice transduced with AAV-Mybpc3 shRNA-1 or shRNA-2. Transcript levels were normalized to expression of the control AAV-LacZ shRNA. Data from three mice per group are presented (mean ± SD). (*D*) Distribution of mononuclear, binuclear, and multinuclear EGFP-expressing myocytes from 4-wk-old wild-type mice transduced (at P1) with AAV-LacZ shRNA (gray), AAV-Mybpc3 shRNA-1 (black), and AAV-Mybpc3 shRNA-2 (white). Data are presented from four mice per genotype, 200–300 cells per mouse (mean ± SD).

DEVELOPMENTAL BIOLOGY

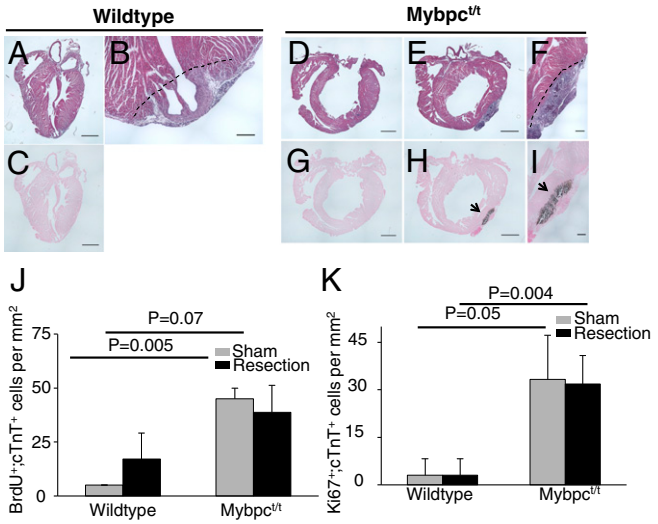

Fig. 5. Cell proliferation in P10 wild-type and Mybpc$^{t/t}$ mice after apical resection. Sections from sham-operated or LV apical resected hearts, 17 d postresection, from wild-type (*A–C*) or Mybpc$^{t/t}$ (*D–I*) mice stained with hematoxylin/eosin (*A*, *B*, and *D–F*) or von Kossa (*C* and *G–I*). Dashed line indicates the resection plane. Note the marked calcium precipitate in apical resected Mybpc$^{t/t}$ (*H* and *I*) but not wild-type (*C*) hearts. [Scale bar, (*A*, *C–E*, *G*, and *H*) 1 mm and (*B*, *F*, and *I*) 200 μm.] Quantification of BrdU-labeled, cTnT-positive myocytes (*J*, BrdU$^+$;cTnT$^+$) and Ki67-positive, cTnT-positive myocytes (*K*, Ki67$^+$;cTnT$^+$) isolated 17 d after sham (gray) or LV apical resection (black) of wild-type and Mybpc$^{t/t}$ mice. Ten sections were counted from each of four mice per genotype, and cell counts are reported as stained cells per mm^2 (mean ± SD).

The findings presented here suggest two independent mechanisms by which *MYBPC3* mutations can alter cardiac morphology. Individuals carrying heterozygous *MYBPC3* mutations develop HCM (46), characterized by cardiac hypertrophy (increased heart mass and altered morphology). These changes in size and shape are due, at least in part, to the increased size of myocytes (hypertrophy) (47). By contrast, individuals homozygous for *MYBPC3* mutations develop cardiac dilation, which we conclude is due to myocyte hyperplasia (increased numbers of myocytes). This myocyte hyperplasia is associated with increased numbers of mononuclear myocytes that may have reduced contractile function. Defining the relationship of homozygous *MYBPC3* DCM to other more common forms of DCM will provide further insights into this clinically important pathophysiology.

Materials and Methods

Mouse Studies. All mouse studies were performed with approved protocols in compliance with the Association for the Assessment and Accreditation of Laboratory Animal Care and Harvard Medical School. Mybpc$^{t/t}$ (16) and wild-type mice (129SvEv background) were studied. The Mybpc$^{t/t}$ alleles contain a PGK-neomycin resistance gene that disrupts exon 30 and is predicted to encode from a truncated peptide that terminates with amino acid residue 1,064 of the 1,270 residues in wild-type cardiac MYBPC. Protein chemical studies have demonstrated that this allele produces less than 10% of the normal amount of cardiac MYBPC.

Myocyte Isolation. Ventricular myocytes were isolated from P1 to P10 mice using a modified collagenase dissociation protocol. After anesthetizing mice [2% (vol/vol) isoflurane inhalation], the thoracic cavity was opened and LV was perfused (2 mL/min) with prewarmed 37 °C buffer (126 mM NaCl, 4.4 mM KCl, 1 mM $MgCl_2$, 4 mM $NaHCO_3$, 30 mM 2,3-butanedione monoxime, 10 mM Hepes, 11 mM Glucose, 0.5 mM EDTA) with 0.09% Collagenase Type I (Worthington), 0.125% Trypsin, and 25 μM $CaCl_2$ for 2 min. The perfused heart was then excised and placed in buffer with 100 μM $CaCl_2$ and 2% BSA for 10 min at 37 °C. Ventricular tissue was minced, and myocytes were dispersed by gentle trituration of minced tissue through a wide bore disposable serologic pipette. The dispersed cells were filtered through a 100 μm nylon mesh and washed twice by centrifugation (50 × *g* for 3 min). The resulting cell pellet was suspended in 1 mL buffer with 100 μM $CaCl_2$ and fixed by the addition of 1 mL 2% (wt/vol) paraformaldehyde in PBS and incubated on ice for 20 min. Fixed myocytes were washed twice in PBS by centrifugation (50 × *g* for 3 min) and stored at 4 °C.

For ventricular myocyte isolation from 3–4-wk-old mice, immediately after sacrifice, hearts were excised, the ascending aorta was quickly cannulated, and the hearts were perfused for 5 min with warm (37 °C) calcium Tyrode's buffer (135 mM NaCl, 4 mM KCl, 0.33 mM NaH_2PO_4, 1.2 mM $MgSO_4$, and 10 mM Hepes, pH 7.40), followed by 10–15 min of perfusion with collagenase B (0.56 mg/mL, Roche), collagenase D (0.48 mg/mL, Roche), and protease XIV (0.07 mg/ml, Sigma). The hearts were minced and filtered as described above. Cells were plated onto laminin-precoated coverslips (1 μg/cm^2; Invitrogen) and cultured for 1 h in MEM (Sigma) containing 10 mM 2,3-butanedione monoxime to extract myocytes from other cardiac cells.

Immunohistochemistry. Histochemical analyses were performed on heart sections fixed in 4% (wt/vol) paraformaldehyde overnight. Sections were treated with xylene (to remove paraffin), rehydrated, and permeabilized in 0.1% (vol/vol) Triton-X100 in PBS. Sections were incubated with primary antibodies applied at 1:200 dilution (unless otherwise indicated) in 0.1% (wt/vol) BSA in PBS overnight at 4 °C, and nonspecific antibody binding was blocked by 1.5% (vol/vol) FCS in PBS. Primary antibodies included the following: BrdU (rat anti-BrdU, Abcam ab6326, 1:200), Ki67 (rabbit anti-Ki67, Abcam ab15580, 1:200), cTnT (mouse anti-cTnT, Abcam ab8295, 1:200), cardiac troponin-I (rabbit anti-Tnni3, Abcam ab56357, 1:200), WGA (Invitrogen W32466, 1:400), pH3 (rabbit anti-pH3, Millipore 06–570, 1:250), and Aurora B (rabbit anti-Aurora B, Abcam ab2254, 1:250). Sections were washed in PBS and fluorophore-conjugated secondary antibody (Molecular Probes) diluted 1:200 in 1% FCS or donkey serum. Nuclei were counterstained with 0.3 μg/mL propidium iodide (Molecular Probes) or 2 μg/mL of 4′,6-diamidino-2-phenylindole (DAPI; Sigma). Myocytes were identified by visualizing sarcomeres with Nomarski (differential interference contrast) light microscope optics and cTnT expression. Fluorescent images of histological sections were captured using the Leica TCS NT confocal microscope system and subsequently analyzed and assembled using Image J and Adobe Photoshop software.

Myocyte Quantification. WGA-stained heart sections were imaged using a Zeiss confocal microscope, and images were processed after color inversion, so that individual cells were highlighted as "particles." The "Watershed" algorithm (Fiji; fiji.sc/) was used to resolve distinct particles that were close together. Particles were included based on the size of cardiomyocytes ranging from 150 to 3,000 pixels/cell.

AAV Production and Purification. AAV vectors were packaged into AAV9 capsid by the triple transfection method using helper plasmids pAdΔF6 and plasmid pAAV2/9 (Penn Vector Core). We used 50 μg of plasmid DNA per 15-cm cell culture plate. Three days after transfection, AAV vectors were purified in Optiprep density gradient medium (D-1556, Sigma) by centrifugation and stored at −80 °C.

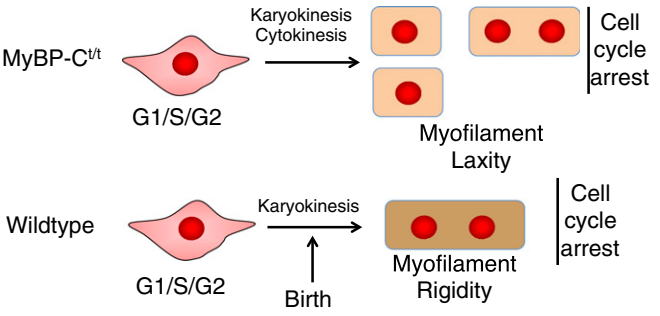

Fig. 6. A schematic of postnatal myocyte development in Mybpc$^{t/t}$ and wild-type mice. In the perinatal period, wild-type myocytes develop dense mature myofibrillar structures as they undergo a final round of DNA replication without cytokinesis, resulting in 95% binuclear myocytes. Mybpc$^{t/t}$ myocytes have reduced myofibrillar density and less rigid sarcomere, prolonged expression of cell cycle markers, resulting in more myocytes and larger proportions of mononuclear myocytes.

shRNA Vector Construction. Two shRNA constructs specific for 21-base-pair sequences corresponding to cardiac *Mypbc3* were constructed. The following targeted sequences were used: Mypbc3-specific shRNA-1, ccagagaaggcagaatctgaa; Mypbc3-specific shRNA-2, aagggtttgcctgcaacctgt; and shRNA control targeting LacZ, gactacacaaatcagcgattt.

RNA-Seq. Hearts from mice were rapidly isolated, placed in room temperature PBS to evacuate blood, and then immersed in RNALater (Qiagen) at room temperature. We used 2 μg of total ventricular RNA to construct RNAseq sequencing libraries (48). At least 20 million 50-bp paired-end DNA reads were obtained from each library using the Illumina HiSeq2500. Data were processed as previously described (48).

Apical Resection. LV apical resection procedures were performed as described (26). In brief, mice were anesthetized on ice to induce deep transient sedation, apnea, and asystole. The thoracic cavity was opened at the fourth intercostal space and the LV exposed. Approximately 15% of the ventricular apex was resected. Successful apical resection was assessed by visualization of the ventricular chamber immediately after resection. Following surgery, mice were rapidly warmed and monitored for viability. Sham-operated mice underwent identical procedures but without LV apex resection. We have independently verified that robust heart regeneration occurs in the neonatal mouse apical resection model (34).

EdU/BrdU Labeling. To assess DNA synthesis in isolated myocytes, neonatal pups received an i.p. injection of EdU (Life Technologies, C10339, 5 mg/kg) for the first 5 d. To label cells with ongoing DNA synthesis, surviving mice subjected to sham or apical-resection surgery received a pulse (two s.c. injections 12 h apart) of BrdU (Sigma, 20 mg/mL solution in sterile PBS, 100 mg/kg dose) on the first day post-resection.

Statistical Analyses. Significance was assessed by two-sample Student's *t* test on selected groups, assuming two-tail heteroscedastic distributions. Multiple group comparison was assessed by ANOVA.

ACKNOWLEDGMENTS. This work was supported in part by funding from NIH Grants 5R01HL080494, 5R01HL084553, and 1U01HL098166 (to C.E.S. and J.G.S.); NIH Grants HL117986 and AG040019 and the Leducq Transatlantic Network (to R.T.L.); NIH Grant F32HL117595 (to C.C.O.); NIH Grants R01HL085487 and R15HL124458 (to B.K.M.); and the Howard Hughes Medical Institute (C.E.S. and J.J.).

1. Maron BJ, et al.; American Heart Association; Council on Clinical Cardiology, Heart Failure and Transplantation Committee; Quality of Care and Outcomes Research and Functional Genomics and Translational Biology Interdisciplinary Working Groups; Council on Epidemiology and Prevention (2006) Contemporary definitions and classification of the cardiomyopathies: An American Heart Association Scientific Statement from the Council on Clinical Cardiology, Heart Failure and Transplantation Committee; Quality of Care and Outcomes Research and Functional Genomics and Translational Biology Interdisciplinary Working Groups; and Council on Epidemiology and Prevention. *Circulation* 113(14):1807–1816.
2. Go AS, et al.; American Heart Association Statistics Committee and Stroke Statistics Subcommittee (2014) Heart disease and stroke statistics—2014 update: A report from the American Heart Association. *Circulation* 129(3):e28–e292.
3. Mann DL, Zipes DP, Libby P, Bonow RO, eds (2014) *Braunwald's Heart Disease: A Textbook of Cardiovascular Medicine* (Elsevier Mosby/Saunders, Philadelphia, PA).
4. Fatkin D, Seidman CE, Seidman JG (2014) Genetics and disease of ventricular muscle. *Cold Spring Harb Perspect Med* 4(1):a021063.
5. McNally EM, Golbus JR, Puckelwartz MJ (2013) Genetic mutations and mechanisms in dilated cardiomyopathy. *J Clin Invest* 123(1):19–26.
6. Mestroni L, Taylor MR (2013) Genetics and genetic testing of dilated cardiomyopathy: A new perspective. *Discov Med* 15(80):43–49.
7. Moss RL, Fitzsimons DP, Ralphe JC (2015) Cardiac MyBP-C regulates the rate and force of contraction in mammalian myocardium. *Circ Res* 116(1):183–192.
8. Gautel M, Fürst DO, Cocco A, Schiaffino S (1998) Isoform transitions of the myosin binding protein C family in developing human and mouse muscles: Lack of isoform transcomplementation in cardiac muscle. *Circ Res* 82(1):124–129.
9. Yin Z, Ren J, Guo W (2015) Sarcomeric protein isoform transitions in cardiac muscle: A journey to heart failure. *Biochim Biophys Acta* 1852(1):47–52.
10. Pfuhl M, Gautel M (2012) Structure, interactions and function of the N-terminus of cardiac myosin binding protein C (MyBP-C): Who does what, with what, and to whom? *J Muscle Res Cell Motil* 33(1):83–94.
11. Ackermann MA, Kontrogianni-Konstantopoulos A (2011) Myosin binding protein-C: A regulator of actomyosin interaction in striated muscle. *J Biomed Biotechnol* 2011:636403.
12. Flashman E, Redwood C, Moolman-Smook J, Watkins H (2004) Cardiac myosin binding protein C: Its role in physiology and disease. *Circ Res* 94(10):1279–1289.
13. Sequeira V, Witjas-Paalberends ER, Kuster DW, van der Velden J (2014) Cardiac myosin-binding protein C: Hypertrophic cardiomyopathy mutations and structure-function relationships. *Pflugers Archiv* 466(2):201–206.
14. Kuster DW, Sadayappan S (2014) MYBPC3's alternate ending: Consequences and therapeutic implications of a highly prevalent 25 bp deletion mutation. *Pflugers Archiv* 466(2):207–213.
15. Dhandapany PS, et al. (2009) A common MYBPC3 (cardiac myosin binding protein C) variant associated with cardiomyopathies in South Asia. *Nat Genet* 41(2):187–191.
16. McConnell BK, et al. (1999) Dilated cardiomyopathy in homozygous myosin-binding protein-C mutant mice. *J Clin Invest* 104(12):1771.
17. Carrier L, et al. (2004) Asymmetric septal hypertrophy in heterozygous cMyBP-C null mice. *Cardiovasc Res* 63(2):293–304.
18. Harris SP, et al. (2002) Hypertrophic cardiomyopathy in cardiac myosin binding protein-C knockout mice. *Circ Res* 90(5):594–601.
19. Mearini G, et al. (2014) Mybpc3 gene therapy for neonatal cardiomyopathy enables long-term disease prevention in mice. *Nat Commun* 5:5515.
20. Merkulov S, Chen X, Chandler MP, Stelzer JE (2012) In vivo cardiac myosin binding protein C gene transfer rescues myofilament contractile dysfunction in cardiac myosin binding protein C null mice. *Circ Heart Fail* 5(5):635–644.
21. Pasumarthi KB, Nakajima H, Nakajima HO, Soonpaa MH, Field LJ (2005) Targeted expression of cyclin D2 results in cardiomyocyte DNA synthesis and infarct regression in transgenic mice. *Circ Res* 96(1):110–118.
22. Soonpaa MH, Kim KK, Pajak L, Franklin M, Field LJ (1996) Cardiomyocyte DNA synthesis and binucleation during murine development. *Am J Physiol* 271(5 Pt 2): H2183–H2189.
23. Snir M, et al. (2003) Assessment of the ultrastructural and proliferative properties of human embryonic stem cell-derived cardiomyocytes. *Am J Physiol Heart Circ Physiol* 285(6):H2355–H2363.
24. Palmer BM, et al. (2004) Effect of cardiac myosin binding protein-C on mechanoenergetics in mouse myocardium. *Circ Res* 94(12):1615–1622.
25. Ahuja P, Sdek P, MacLellan WR (2007) Cardiac myocyte cell cycle control in development, disease, and regeneration. *Physiol Rev* 87(2):521–544.
26. Porrello ER, et al. (2011) Transient regenerative potential of the neonatal mouse heart. *Science* 331(6020):1078–1080.
27. Soonpaa MH, et al. (1997) Cyclin D1 overexpression promotes cardiomyocyte DNA synthesis and multinucleation in transgenic mice. *J Clin Invest* 99(11):2644–2654.
28. Bradford JA, Clarke ST (2011) Dual-pulse labeling using 5-ethynyl-2′-deoxyuridine (EdU) and 5-bromo-2′-deoxyuridine (BrdU) in flow cytometry. *Curr Protoc Cytom* Chapter 7:Unit 7.38.
29. Gerdes J, et al. (1984) Cell cycle analysis of a cell proliferation-associated human nuclear antigen defined by the monoclonal antibody Ki-67. *J Immunol* 133(4):1710–1715.
30. Poon RY (2013) Aurora B: Hooking up with cyclin-dependent kinases. *Cell Cycle* 12(7): 1019–1020.
31. Prasad KM, Xu Y, Yang Z, Acton ST, French BA (2011) Robust cardiomyocyte-specific gene expression following systemic injection of AAV: In vivo gene delivery follows a Poisson distribution. *Gene Ther* 18(1):43–52.
32. Gao G, Vandenberghe LH, Wilson JM (2005) New recombinant serotypes of AAV vectors. *Curr Gene Ther* 5(3):285–297.
33. Jiang J, Wakimoto H, Seidman JG, Seidman CE (2013) Allele-specific silencing of mutant Myh6 transcripts in mice suppresses hypertrophic cardiomyopathy. *Science* 342(6154):111–114.
34. Bryant DM, et al. (2015) A systematic analysis of neonatal mouse heart regeneration after apical resection. *J Mol Cell Cardiol* 79:315–318.
35. Michalek AJ, et al. (2013) Phosphorylation modulates the mechanical stability of the cardiac myosin-binding protein C motif. *Biophys J* 104(2):442–452.
36. Palmer BM, et al. (2011) Roles for cardiac MyBP-C in maintaining myofilament lattice rigidity and prolonging myosin cross-bridge lifetime. *Biophys J* 101(7):1661–1669.
37. Previs MJ, Beck Previs S, Gulick J, Robbins J, Warshaw DM (2012) Molecular mechanics of cardiac myosin-binding protein C in native thick filaments. *Science* 337(6099):1215–1218.
38. Ahuja P, Perriard E, Perriard JC, Ehler E (2004) Sequential myofibrillar breakdown accompanies mitotic division of mammalian cardiomyocytes. *J Cell Sci* 117(Pt 15): 3295–3306.
39. Li F, Wang X, Capasso JM, Gerdes AM (1996) Rapid transition of cardiac myocytes from hyperplasia to hypertrophy during postnatal development. *J Mol Cell Cardiol* 28(8):1737–1746.
40. Li F, Wang X, Gerdes AM (1997) Formation of binucleated cardiac myocytes in rat heart: II. Cytoskeletal organisation. *J Mol Cell Cardiol* 29(6):1553–1565.
41. Poolman RA, Li JM, Durand B, Brooks G (1999) Altered expression of cell cycle proteins and prolonged duration of cardiac myocyte hyperplasia in p27KIP1 knockout mice. *Circ Res* 85(2):117–127.
42. Kosaka Y, et al. (2012) 14-3-3ε plays a role in cardiac ventricular compaction by regulating the cardiomyocyte cell cycle. *Mol Cell Biol* 32(24):5089–5102.
43. Mahmoud AI, et al. (2013) Meis1 regulates postnatal cardiomyocyte cell cycle arrest. *Nature* 497(7448):249–253.
44. Puente BN, et al. (2014) The oxygen-rich postnatal environment induces cardiomyocyte cell-cycle arrest through DNA damage response. *Cell* 157(3):565–579.
45. Kulikovskaya I, McClellan GB, Levine R, Winegrad S (2007) Multiple forms of cardiac myosin-binding protein C exist and can regulate thick filament stability. *J Gen Physiol* 129(5):419–428.
46. Morita H, Seidman J, Seidman CE (2005) Genetic causes of human heart failure. *J Clin Invest* 115(3):518–526.
47. Marston S, et al. (2009) Evidence from human myectomy samples that MYBPC3 mutations cause hypertrophic cardiomyopathy through haploinsufficiency. *Circ Res* 105(3):219–222.
48. Christodoulou DC, et al. (2014) 5′RNA-Seq identifies Fhl1 as a genetic modifier in cardiomyopathy. *J Clin Invest* 124(3):1364–1370.